

Effect of Nanocrystalline Structure on the Corrosion of a Fe20Cr Alloy

Rajeev K. Gupta^{1,2,3*}, R.K. Singh Raman^{1,4}, Carl C. Koch⁵, B.S. Murty⁶

¹ Dept. of Mechanical and Aerospace Engineering, Monash University, Victoria 3800, Australia

² Dept. of Materials Engineering, Monash University, Victoria 3800, Australia

³ Institute for Frontier Materials, Deakin University, Victoria 3216, Australia

⁴ Dept. of Chemical Engineering, Monash University, Victoria 3800, Australia

⁵ Dept. of Materials Science and Engineering, North Carolina State University, USA

⁶ Dept. of Metallurgical and Materials Engineering, Indian Institute of Technology Madras, Chennai, India 600036

*E-mail: r.gupta@deakin.edu.au

Received: 13 October 2012 / Accepted: 3 April 2013 / Published: 1 May 2013

The corrosion behaviour of nanocrystalline and microcrystalline Fe20Cr alloys, prepared by high energy ball milling followed by compaction and sintering, was studied in 0.05M H₂SO₄ and 0.05M H₂SO₄ + 0.5M NaCl by potentiodynamic polarization. The nanocrystalline alloy exhibited improved passivating ability and pitting resistance as described by passivation potential, critical current density, passive current density and breakdown potential. XPS and SIMS analysis revealed greater Cr content in the passive film formed on the nanocrystalline form of the alloy. The enhanced passivating ability of the nanocrystalline alloy was attributed to the formation of the passive film with higher Cr content.

Keywords: Stainless steel; polarization; XPS; Passive films, Passivity; Interfaces; Nanocrystalline

1. INTRODUCTION

Recently, special attention has been paid to investigate nanocrystalline (nc) materials as they exhibit different and often improved properties over conventional microcrystalline (mc) materials of the same chemical composition [1-4]. The corrosion behaviour of nc materials has also attracted significant attention of the research community and recently reviewed by Ralston and Birbilis [5]. The effect of nanocrystalline structure on the corrosion behaviour of a material was found to depend on its composition as well as on the corrosion media [5]. Generally, a nanocrystalline structure is expected to accelerate the corrosion rate of an active material because of a drastic increase of grain boundaries [5].

On the other hand, nanocrystalline structure can improve the corrosion resistance of a passive alloy by forming a more protective passive film [5].

Fe-Cr alloys are well known for their good corrosion resistance owing to the formation of a Cr rich passive film [6-8]. Nanocrystalline structure may impart significant improvement in corrosion performance of a Fe-Cr alloy by enhancing the Cr content of the passive film developed upon it. However, effect of nanocrystalline structure on the corrosion performance of Fe-Cr alloys is contradictory and both improvement and deterioration of corrosion performance due to nanocrystalline structure are reported in the literature [5]. Improved corrosion performance of nc Fe-Cr alloys was explained mainly on the basis of greater Cr enrichment of the passive film formed on the nc structure due to faster diffusion of Cr [9,10]. Formation of a relatively more homogenous, compact passive film with improved adhesion was the additional factor attributed to the improved corrosion performance of nanocrystalline Fe-Cr alloys [10-12]. Investigations reporting deterioration of corrosion performance caused by nanocrystalline structure proposed the higher reactivity, residual stresses and defects to be the main attributes [12,13].

It is interesting to note that the processing routes employed for developing a nanocrystalline structure in steels described above were considerably different from those employed for producing microcrystalline alloy to which they were compared. Processing employed to produce nanocrystalline Fe-Cr alloys lead to microstructural changes (i.e., internal stresses, development of alloy texture, solute segregation, phase transformation etc.) in addition to grain refinement, which can also affect the corrosion response. In fact, in one of the studies [11], showing improved corrosion resistance of nc steel coating over mc steel, the microstructure of the nc steel was described to be ferritic, whereas that of the mc steel to be austenitic and as a result the observed difference in the corrosion performance might have been influenced by different phases present in nc and mc test specimen. Moreover, the nanocrystalline surfaces used for the corrosion studies were in the form of thin surface films. Therefore, it may not be inappropriate to suggest that the effects of nanocrystalline structure on the corrosion of steel, as claimed in the studies discussed earlier, could also be dominated by factors (i.e., such as residual stresses, solute segregation, phase composition and other defects present) other than the nanocrystalline structure.

Literature suggests that the process used to produce nanocrystalline surfaces may cause significant chemical and physical changes in addition to the grain refinement [14]. As such, in the light of issues described above, for the investigation of role of nanocrystalline structure on the corrosion behaviour of Fe-Cr alloys, it is necessary to produce the test specimen with the grain size in two distinct sizes by similar route. As such, Fe20Cr alloy test specimens used in the current study were prepared by ball-milling followed by annealing, compaction and sintering; to the best of authors' knowledge this is the first study addressing the passivation behaviour of ball-milled nanocrystalline Fe-Cr based alloys.

In addition to the controversy on the effect of nanocrystalline structure on the corrosion performance of alloys, a mechanism for the improvement or deterioration of corrosion performance due to a nanocrystalline structure is also not well established in the literature for steels. The investigations reporting enhancement in corrosion performance of nanocrystalline steels have been attributed to the surface enrichment of the Cr caused by enhanced diffusivity of Cr in nanocrystalline

structure [9,10]. However, none of the investigations compared the chemical composition of the corrosion films developed on nano and microcrystalline Fe-Cr based alloys to show greater surface enrichment of Cr in nanocrystalline alloys experimentally. In the present investigation, the chemical composition of the corrosion films developed on the nano and microcrystalline Fe₂₀Cr alloys was analysed for the first time using X-ray photoelectron spectroscopy (XPS) and secondary ion mass spectrometry (SIMS) and possible mechanisms of the enhanced surface enrichment of Cr in nc FeCr alloys were proposed.

2. EXPERIMENTAL PROCEDURE

2.1. Sample preparation and characterization

A Fe-Cr alloy with a nominal Cr content of 20 wt.% was prepared by mechanical alloying. As starting materials, high purity powders of Fe (99.9% purity and particle size <10 μm) and Cr (99.9% and particle size <10 μm) were loaded into a tool steel vial under vacuum with 440C stainless steel balls (6.4–7.9 mm in diameter). Ball-to-powder weight ratio was kept at 10:1. High-energy ball milling was carried out for 20 h in SPEX Model 8000 shaker mill which was air-cooled. The ball-milled alloy powders were annealed at 600 °C in a forming gas atmosphere (98% Ar + 2% H₂) for different times ranging between 3 and 90 min. As-milled and annealed samples were compacted into pellets (diameter = 12 mm and thickness = 1.5 mm) under a uni-axial pressure of 3 GPa. Density of the pellets (before and after sintering) was measured by gas pycnometry. X-ray diffraction (XRD) was performed on the as-milled, annealed and compacted samples with a Cu K α radiation ($\lambda = 0.1541$ nm) at a scan rate of 0.3°/min, and at 50 steps per degree. Grain size of the nanocrystalline alloy after various stages of processing was determined from the X-ray peak broadening using the Voigt function [15,16], after eliminating the instrumental and lattice strain contributions to peak broadening. The four most intense peaks (1 1 0, 2 0 0, 2 1 1, 2 2 0) were used to calculate the grain size. In order to ensure reproducibility, several annealing treatments and the X-ray analyses were duplicated. The accuracy of the grain size determination was within ± 4 nm.

The grain size of nc and mc compacted test specimens was also verified using transmission electron microscope (TEM). TEM samples were prepared by grinding of test specimens up to a thickness of ~ 80 μm followed by ion milling. The ion-milled TEM specimens were analyzed in dark field and selected area diffraction modes using Philips CM20 transmission TEM. An acceleration voltage of 200 kV was used in all the experiments.

2.2 Corrosion testing

The test specimens (pellets of nc and mc Fe-20Cr alloy) were polished to 2500-grit paper finish, cleaned and subjected to potentiodynamic polarization tests. A conventional three-electrode electrochemical cell was used, with the Fe-Cr alloy samples as working electrode (test specimen), a graphite rod as counter electrode and a saturated calomel electrode (SCE) as the reference electrode.

All the potentials, reported in this study, are with respect to SCE. Potentiodynamic polarization tests were carried out at room temperature in 0.05M H₂SO₄ and 0.05M H₂SO₄+ 0.5M NaCl solutions using PAR-2273 potentiostat, employing a scan rate of 0.5 mV/sec. Prior to all experiments, the working electrode was cathodically polarized at -1.0 V for 120 s to remove any existing oxide film. Open circuit potential was monitored for 30 min. to confirm its stability with time. Any fluctuation of the open circuit potential less than 10 mV in a period of 1000 s was considered as a stable potential for carrying out the corrosion tests. These experiments were repeated at least five times to ensure the reproducibility of the data.

2.3 SIMS and XPS

XPS and SIMS analysis was carried out to compare the Cr content of passive films developed on nc and mc Fe₂₀Cr alloys. In order to prepare the samples for XPS analysis, Fe-Cr alloys were polarized (from open circuit) to the potential in the middle of the passivation range (300 mV_{SCE} in 0.05M H₂SO₄ and -190 mV_{SCE} in 0.05M H₂SO₄+ 0.5M NaCl) and held at that potential until a stable current was reached (which took 30 minutes). Samples were then washed with distilled water and ethanol and dried in air at room temperature. Corrosion films thus produced were analysed using a Kratos Axis Ultra Spectrometer with monochromatized Al K_α (1486.6 eV). A charge neutralizer was employed to minimize the photoemission charging effect. Quantitative analysis was performed using Casa-XPS software. The survey scans were generated under the conditions: energy range: 1600-0 eV, pass energy= 160 eV, step size=0.7 eV, sweep time= 180 sec and x-ray spot size=700×300 μm.

Sample preparation for SIMS was similar to XPS and passive film was characterised using a Cameca ims (5f) dynamic SIMS instrument. Craters of 250× 250 μm were analysed using Cs⁺ ion primary beam (2 nA).

3. RESULTS

3.1. Preparation and characterization of test specimens

Nanocrystalline Fe₂₀Cr alloy as produced by high-energy ball milling was initially in the form of powder with an average grain size of 14 nm. The details of the method of consolidation without excessive grain growth are given in an earlier report of the present authors [16]. A systematic study [16] of the grain growth behaviour of a ball milled nc Fe-10Cr alloy powder over a wide range of time and temperature, suggested 600°C to be the optimum temperature for the consolidation of a nc Fe10Cr alloy.

Grain growth behaviour of Fe₂₀Cr alloy at 600°C (Figure 1) was very similar to that of Fe-10Cr alloy and hence a temperature of 600°C was employed for the consolidation of nc Fe₂₀Cr alloy. A schematic representation of the process used for the consolidation is presented in Figure 2. An additional step of annealing prior to compaction made the consolidation possible with available experimental facilities as hardness decreased from 9.2 GPa to 6.8 GPa (Figure 1) while the grain size

increased from 14 nm to 43 nm (which is still in nanocrystalline regime). Compacted pellets were sintered at 600°C for 60 min.

Microcrystalline Fe₂₀Cr alloy test specimens were prepared by sintering the nanocrystalline test specimen (prepared as described earlier) at 840°C for three hours. Grain size and density measured at each steps of processing are presented Table 1.

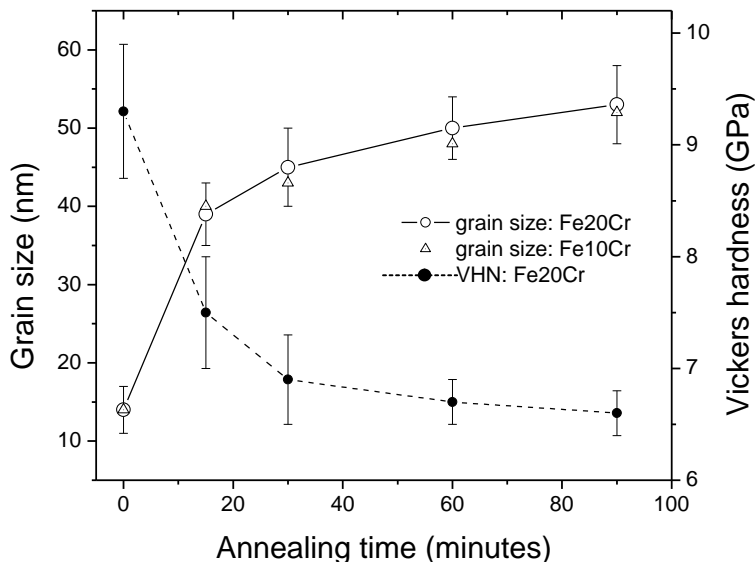


Figure 1. Grain size and hardness of a ball milled Fe₂₀Cr alloy versus annealing time at 600°C. Grain size of Fe₁₀Cr [16] is plotted along with the grain size of Fe₂₀Cr alloy.

Table 1. Grain size and density of nanocrystalline Fe₂₀Cr alloys after different processing steps

	Grain size, ball-milled powder (nm)	Annealing, ball-milled powder	Grain size, ball-milled and annealed powder (nm)	Green density of compacted pellets (% of theoretical density)	Sintering, compacted pellets	Grain size, sintered pellet (nm)	Sintered density of compacted pellets (% of theoretical density)
nc Fe ₂₀ Cr	14(±4)	600°C, 30 min	43 (±4)	98.6 (±0.6)	600°C, 60 min	53(±4)	99.4 (±0.3)
mc Fe ₂₀ Cr	14(±4)	600°C, 30 min	43 (±4)	98.6 (±0.6)	840°C, 180 min	1500 (±200)	99.6 (±0.3)

Grain size of nc test specimen as determined using XRD was found to be 53 (±4) nm whereas that of microcrystalline test specimen as determined using optical microscopy was found to be 1.5 (±0.2) μm. XRD profiles, as presented in the Figure 3, confirm ferritic crystal structure in both

nanocrystalline and microcrystalline test specimen. Nanocrystalline structure of Fe₂₀Cr alloy as determined by XRD was further verified using TEM (Figure 4).

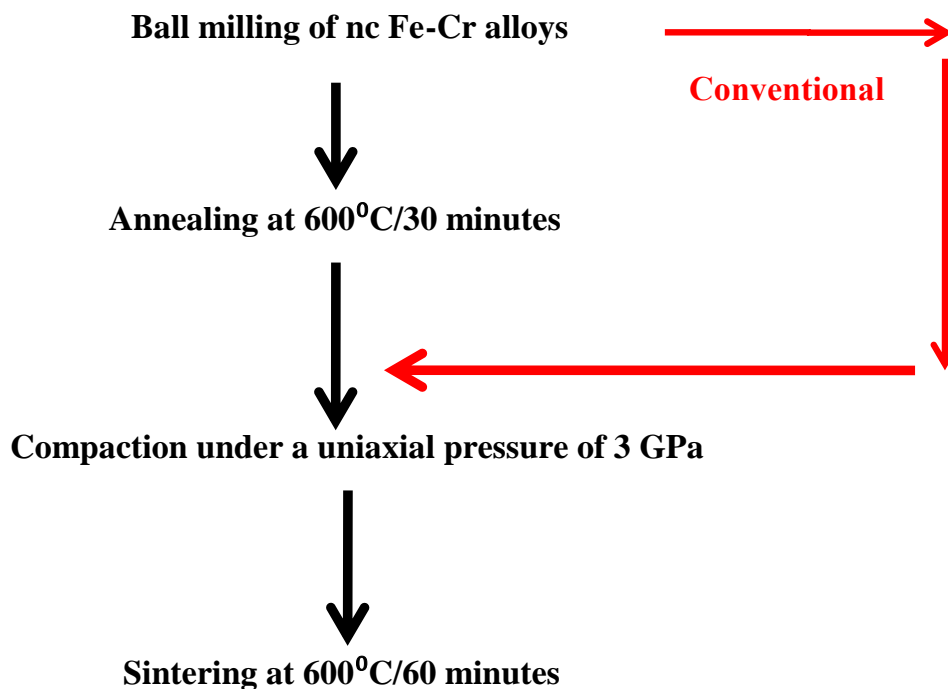


Figure 2. Schematic representation of process used for preparation of a nc Fe₂₀Cr alloy test specimen. Arrow shown in the red indicates the conventional compaction method.

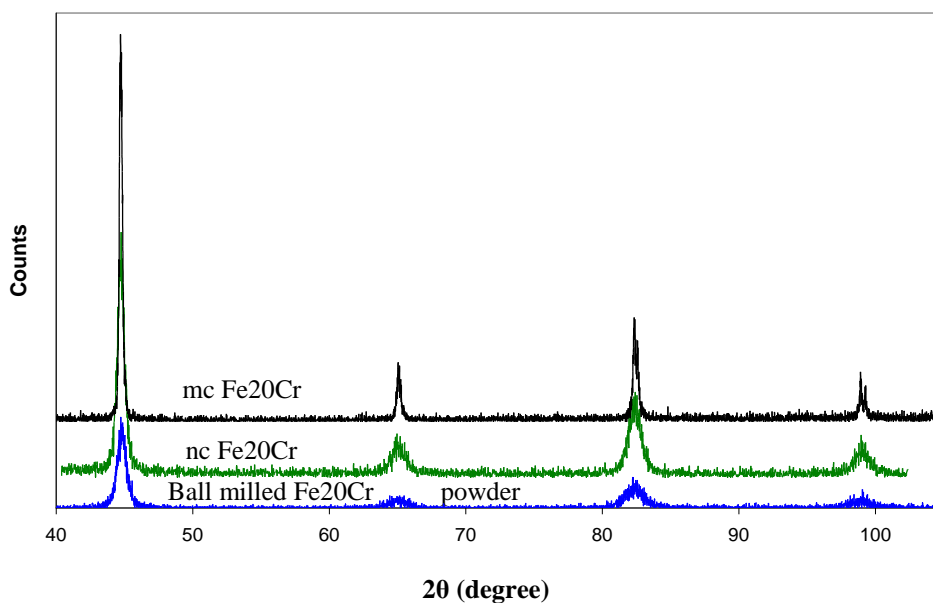


Figure 3. XRD patterns of nc Fe₂₀Cr and mc Fe₂₀Cr test specimens, showing same phases present in the nc and mc Fe₂₀Cr alloys. Peak broadening decreases and peak intensity increases with increase the grain size.

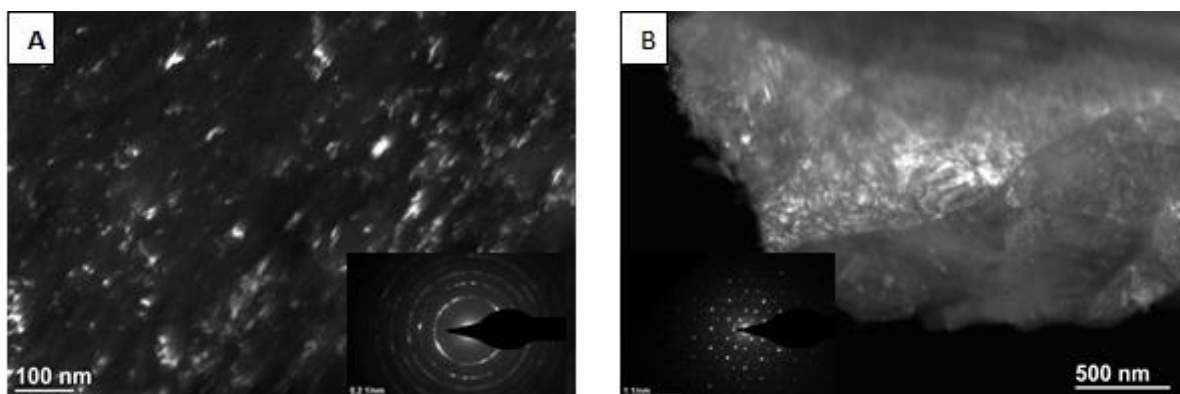


Figure 4. Dark field TEM images of A) nc and B) mc Fe20Cr tests specimens. Selected area diffraction pattern is shown in the inset.

3.2 Potentiodynamic polarization tests

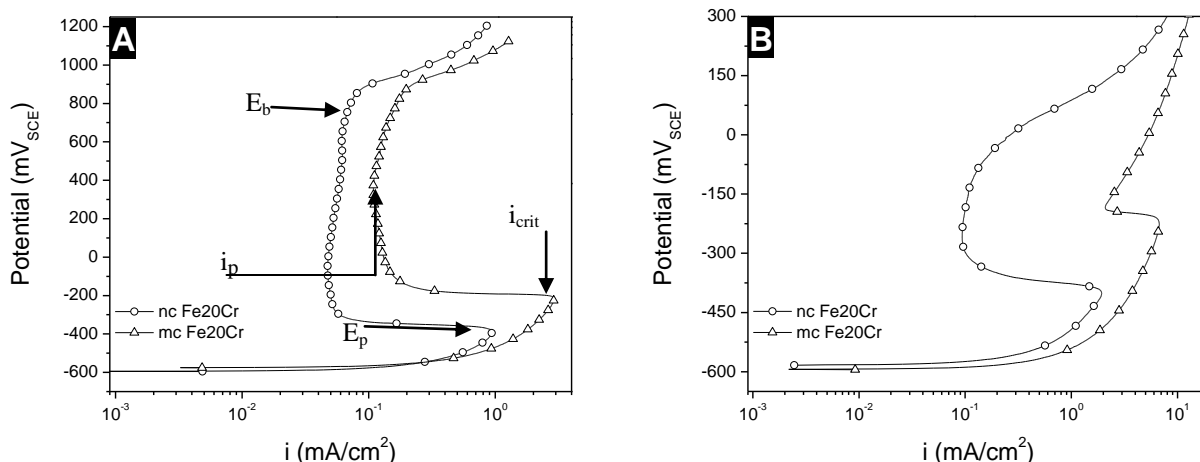


Figure 5. Anodic polarization curves of nc and mc Fe20Cr in: A) 0.05M H₂SO₄ solution and B) 0.05M H₂SO₄ + 0.5M NaCl solution

Potentiodynamic polarization curves obtained for nc and mc Fe20Cr alloys in 0.05M H₂SO₄ and 0.05M H₂SO₄ + 0.5M NaCl solutions are presented in Figure 5(a) and 5(b), respectively. Various parameters (i.e., passivation potential, passive current density, critical current density and breakdown potential) used to describe the passivating ability are described in the Figure 5 and are summarized in the Table 2.

Passivating ability of Fe20Cr alloy, as indicated by negative shift of passivation potential and significant decrease in the anodic current densities, was improved significantly by the grain refinement to nanometer level. Passivation potential (*E_p*) of nanocrystalline Fe20Cr alloy was 180 (±15) mV more negative than that of mc Fe20Cr alloy in both solutions. Critical current density (*i_{crit}*) and passive current density (*i_p*) of nc Fe20Cr alloy were less than those of mc Fe20Cr alloy.

Table 2. Electrochemical data from anodic polarization tests of nc Fe20Cr and mc Fe20Cr alloys. Reported data (E_{corr} : corrosion potential, E_p : passivation potential, E_b : breakdown potential, i_{crit} critical current density and i_p : passive current density) is an average of at least five experimental results, error shown in the brackets is standard deviation

Test Material/Electrolyte	E_{corr} (mV _{SCE})	E_p (mV _{SCE})	E_b (mV _{SCE})	i_p ($\mu\text{A}/\text{cm}^2$)	i_{crit} (mA/cm^2)
nc Fe20Cr/0.05M H ₂ SO ₄	-590 (± 5)	-400 (± 5)	880(± 8)	50(± 5)	0.85 (± 0.1)
mc Fe-20C/0.05M H ₂ SO ₄	-590 (± 5)	-220 (± 15)	880(± 8)	91(± 10)	3.4 (± 0.8)
nc Fe20Cr/0.05M H ₂ SO ₄ +0.5NaCl	-590 (± 5)	-395 (± 3)	-70 (± 15)	100 (± 10)	1.5 (± 0.3)
mc Fe20Cr/0.05M H ₂ SO ₄ +0.5NaCl	-590 (± 5)	-205 (± 25)	-189 (± 40)	1000 (± 500)	8.41(± 1.3)

Addition of chloride ions did not affect the passivation potential of nc and mc Fe20Cr alloys much, albeit shifted the breakdown potential of both the alloys in negative direction. Interestingly, negative shift in the breakdown potential of nc alloy was not as pronounced as that of mc alloy. Nanocrystalline alloy showed an appreciable passive region ($E_{\text{pp}}-E_b=325$ mV) whereas passive region ($E_{\text{pp}}-E_b=16$ mV) in mc Fe20Cr alloy was not well defined in presence of chloride ions. Superior pitting resistance of nanocrystalline alloy over its microcrystalline counterpart was shown clearly by polarization tests in presence of chloride ions.

3.3 Potentiostatic polarization

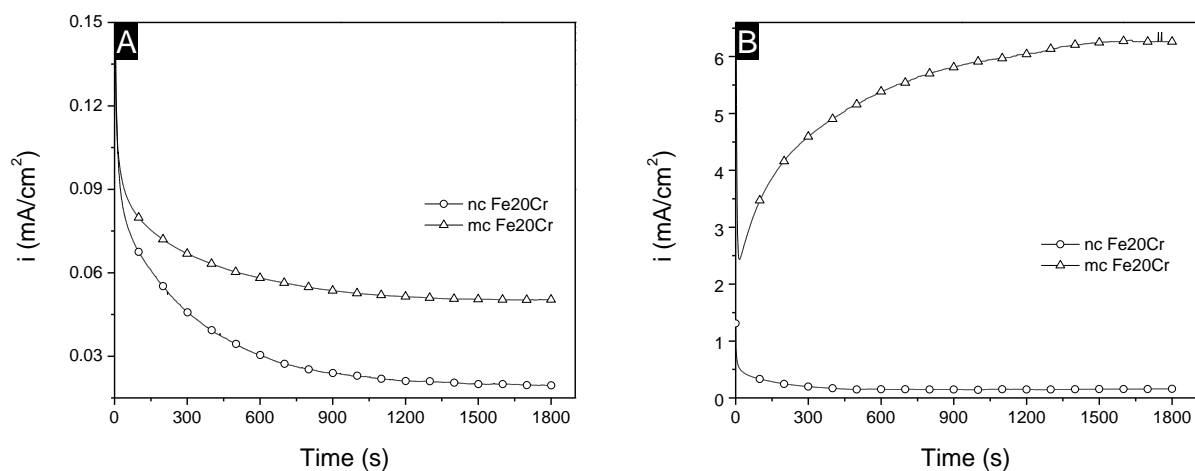


Figure 6. Potentiostatic polarization curves of nc and mc Fe20Cr alloys in: A) 0.05M H₂SO₄ at 300 mV_{SCE} and B) 0.05M H₂SO₄ + 0.5M NaCl solution at -190 mV_{SCE}. Prior to potentiostatic polarization, each of the samples was polarized potentiodynamically at a scan rate of 0.5 mV/sec to the potential where it was held for 30 minutes under potentiostatic control.

Table 3. Atomic ratio of Cr ($\text{Cr}/(\text{Fe}+\text{Cr})$) in the passive film of nanocrystalline (nc) and microcrystalline (mc) Fe₂₀Cr alloy. $i_{\text{steady state}}$ is the steady state current density after 30 minutes of potentiostatic polarization as shown in Figure 6

Test Material/Electrolyte	Applied potential	$i_{\text{steady state}}$ ($\mu\text{A}/\text{cm}^2$)	Cr/(Fe+Cr)
nc Fe ₂₀ Cr/0.05M H ₂ SO ₄	300 mV _{SCE}	20	0.73
mc Fe-20C/0.05M H ₂ SO ₄	300 mV _{SCE}	49	0.62
nc Fe ₂₀ Cr/0.05M H ₂ SO ₄ +0.5NaCl	-190 mV _{SCE}	82	0.45
mc Fe ₂₀ Cr/0.05M H ₂ SO ₄ +0.5NaCl	-190 mV _{SCE}	6200	0.25

Nanocrystalline and mc Fe₂₀Cr alloys were polarized potentiodynamically to 300 mV (in 0.05M H₂SO₄) and held at this potential for 30 minutes in order to develop passive film for compositional characterization. Current density appeared in the two alloys during potentiostatic polarization at 300 mV as presented in Figure 6a and Table 3 showed that nanocrystalline alloy possessed lower current density than microcrystalline alloy for whole period of potentiostatic polarization. Similarly, current was recorded as function of time in 0.05M H₂SO₄ + 0.5 M NaCl for both the alloys at an applied potential of -190 mV. Current density in nanocrystalline alloy decreased with time whereas that in mc alloy increased with time indicating no passivation of mc Fe₂₀Cr alloy in presence of 0.5M chloride ions (Figure 6b and Table 3).

3.4 Compositional analysis of passive film using SIMS

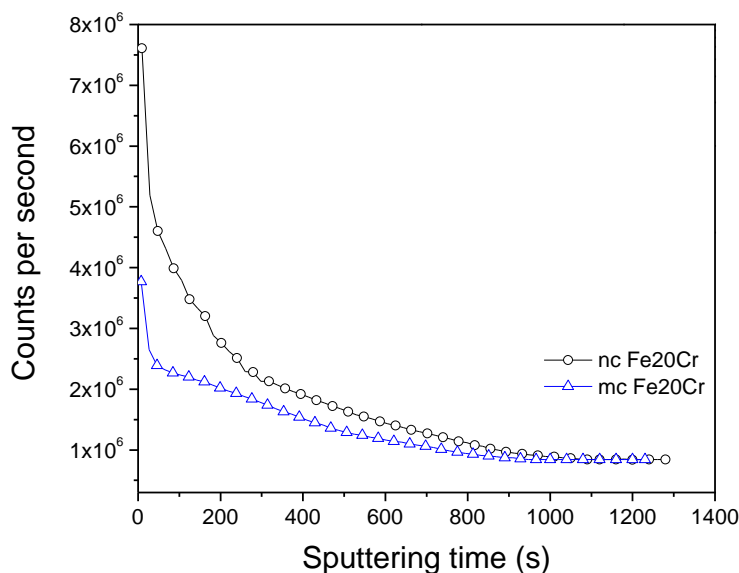


Figure 7. SIMS depth profile for Cr in the passive film developed upon nanocrystalline (nc) and microcrystalline (mc) Fe₂₀Cr alloys after potentiostatic polarization at 300 mV_{SCE} for 30 minutes.

SIMS depth profiling was used to compare the Cr content of the passive films developed upon nc and mc Fe₂₀Cr alloys in 0.05M H₂SO₄ solution (as described in section 3.3). Cr SIMS depth profiles thus obtained (Figure 7) suggested that passive film developed on nc Fe₂₀Cr alloy was richer in Cr than that of mc Fe₂₀Cr alloy. With the progress of sputtering (as the base alloy approached), Cr content decreased and became equal to that in the base alloy (Figure 7).

3.5 Compositional analysis of passive film using XPS

Chemical composition of the passive film developed on nc and mc Fe₂₀Cr alloys was quantified using XPS. Atomic ratio of Cr with respect to combined Fe and Cr (i.e., Cr/(Fe+Cr)) were calculated using the atomic fractions obtained from the survey scans and are presented in Table 3.

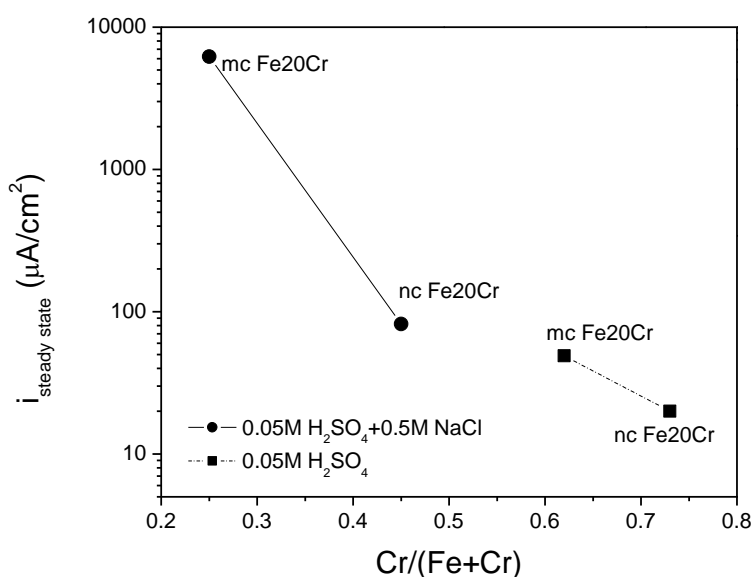


Figure 8. Steady state current densities and Cr content of the passive films developed upon nc and mc Fe₂₀Cr alloys during potentiostatic polarization in the two solutions.

Passive film developed on nc form of the Fe-Cr alloy had significantly higher Cr to (Fe+Cr) ratio in comparison to that in its mc counterpart (Table 3). Atomic ratio of Cr in nc and mc Fe₂₀Cr alloys (without any electrochemical treatment) was 0.21, whereas, XPS analysis of the corrosion film suggested significant Cr enrichment of the corrosion film. The atomic ratio of Cr for the passive film of nc (0.73) and mc (0.62) alloy in 0.05M H₂SO₄ were considerably higher than the base alloy (0.21).

Addition of chloride ions decreased the Cr content of the corrosion film substantially as the Cr to (Fe+Cr) ratio obtained in the corrosion film of nc Fe₂₀Cr in 0.05M H₂SO₄ + 0.5M NaCl was ~0.45 and that of mc alloy was ~0.25 (Table 3). The corrosion film developed upon the microcrystalline alloy showed effectively no Cr enrichment of the corrosion film and therefore no passivation.

Figure 8 shows the variation of Cr content of the passive films with the steady state current densities after the potentiostatic polarization of two alloys for 30 minutes in nc Fe₂₀Cr in 0.05M

H₂SO₄ + 0.5M NaCl. Nanocrystalline alloy exhibited significantly lower steady state current density and higher Cr content of the passive film in both the solutions.

4. DISCUSSION

4.1. Enhanced passivity of nanocrystalline Fe20Cr alloy

This investigation has established a significant improvement in the passivating ability and pitting resistance of Fe20Cr alloy caused by the grain refinement to nanometer level. These findings are consistent with a few other findings performed on various nanocrystalline steels [9-11]. Significant negative shift in the passivation potential caused by nanocrystalline structure can be understood due to combined effect of increased surface reactivity and higher Cr enrichment of the passive film. Passivation potential can be calculated from the free enthalpy of the reaction of formation of passive oxide or oxy-hydroxide according to the following equation [6]:

$$E_p = \frac{G_p}{2F} \quad (1)$$

where, G_p is the free enthalpy of the reaction of passive oxide formation (per mol oxide) and F is Faraday's constant.

If the corresponding free enthalpy for formation of passive film on a FeCr alloy is assumed to be linear combination of the values of pure elements according to the composition of the precursor, then

$$G_p = x_{Cr}G_{Cr} + (1 - x_{Cr})G_{Fe} \quad (2)$$

where, G_{Cr} and G_{Fe} are the free enthalpies of the formation of the Cr and Fe oxides respectively and x_{Cr} is fraction of Cr present on the electrolyte/alloy interface. Passivation potential of the a Fe-Cr alloy can be obtained by combining equation 1 and 2 as:

$$E_p = x_{Cr}E_{p,Cr} + (1 - x_{Cr})E_{p,Fe} \quad (3)$$

Equation 3 indicates that passivation potential of a Fe-Cr alloy depends not only upon the individual passivation potential but also upon the Cr concentration of the alloy. Equation 3 was used by Kirchheim et al [17] to determine the passivation potential of various Fe-Cr alloys in sulphuric acid solution. In the current study, Cr concentration of passive film formed in nanocrystalline alloy was found to be higher than that of microcrystalline alloy (as shown by SIMS and XPS data). According to equation 3, a higher Cr concentration developed in the nanocrystalline alloy may have shifted the potential in the negative direction.

Nanocrystalline alloys are reported to have more free energy caused by higher fraction of grain boundary and triple points and therefore should have more negative value of free enthalpy of reaction

occurring on them [18-20]. This indicates that nanocrystalline structure will lead to more negative passivation potential according to equation 1. In fact, more negative passivation potential caused by nanocrystalline structure is reported in many passive metals [21,22] and even in Fe [23-26]. A negative shift in individual E_p of Cr and Fe due to nanocrystalline structure will lead to more negative E_p of nanocrystalline Fe20Cr alloy.

4.2. Enhanced Cr enrichment

Improvement in the passivating ability and pitting resistance of nanocrystalline Fe20Cr alloy can be attributed to increased Cr content of the passive film formed on nanocrystalline alloys which is evident from both SIMS and XPS analysis in the current study. Various authors have proposed that the Cr enrichment of the passive film was caused by faster diffusion of Cr from the bulk alloy to passive film/alloy interface. This explanation is possible at elevated temperatures because of faster diffusion of Cr. Authors previous work has also shown improvement of the oxidation resistance of nanocrystalline Fe-Cr alloys at elevated temperature (400°C) due to enhanced diffusion of Cr [4]. However, the view of faster diffusion of Cr from bulk material to the interface of bulk material/corrosion film at room temperature does not seem plausible because of very low diffusivity of Cr at room temperature. Grain boundary diffusion coefficient (D_{gb}) of Cr in BCC Fe at room temperature is $4.1 \times 10^{-40} \text{ m}^2/\text{s}$. and lattice diffusion coefficient (D_b) is even lower, i.e., $9.4 \times 10^{-48} \text{ m}^2/\text{s}$ (diffusion coefficients were derived upon extrapolation of the reported diffusion data at higher temperatures [27-29]). Assuming the effective diffusion coefficient D can be expressed as the linear combination of grain boundary and lattice diffusion coefficients as following:

$$D = fD_{gb} + (1-f)D_b \quad (4)$$

where f , grain boundary fraction can be represented as [30]:

$$f = \frac{3\delta(d-\delta)^2}{d^3} \quad (5)$$

d is the grain size and δ is the grain boundary thickness. Using equation 4 and 5 the diffusion coefficient can be calculated as a function of grain size. Diffusion coefficient of Cr for nanocrystalline alloys with a grain size of 10 nm (assuming grain boundary width to be 1 nm) was calculated to be $1.2 \times 10^{-40} \text{ m}^2/\text{s}$ and that of fine grain material with grain size of 5 μm was $8 \times 10^{-43} \text{ m}^2/\text{s}$. At this low diffusion coefficients; transport of Cr from the bulk to corrosion film/metal interface (and therefore Cr enrichment of corrosion film) does not seem feasible and therefore an alternative explanation for Cr enrichment of passive film is required.

It seems possible to explain the higher Cr content of the passive film formed on nanocrystalline Fe-Cr alloys on the basis of the combined role of nanocrystalline structure and oxidation potentials of Cr and Fe in the formation (or lack of formation) of passive layers with Cr enrichment. One of the theories for the passivity of stainless steels is based on the selective dissolution of Fe and formation of

Cr oxide layer in the potential regime where Cr form stable Cr-oxide whereas Fe will dissolve [17,31-35]. This is possible because the passivation potential of Cr is considerably more negative than for Fe. However, in the potential regime where Cr oxidizes to form protective oxide but Fe undergoes dissolution, any factor that may facilitate surface reactivity will aid to both the processes (i.e., Cr-rich oxide film formation and Fe dissolution). Nanocrystalline surfaces, due to high fraction of grain boundaries and triple points, are considerably more reactive than microcrystalline surfaces [2,18,30]. Consequently, the simultaneous dissolution of Fe and formation of Cr-oxide layer was accelerated leading to enhanced Cr content of the passive film.

4.3. Enhancement of pitting resistance in presence of chloride ions

Chloride ions caused a significant increase in the measured anodic current density and a negative shift in the breakdown potential [6]. Despite of same Cr content, pitting resistance (as expressed by anodic current densities and breakdown potential) of nanocrystalline alloy remained superior to that of the microcrystalline alloy. This can be explained on the basis of formation of passive layer richer in Cr which offers improved resistance to disruption in the passivity by Cl⁻ ions [6,35] and therefore nanocrystalline Fe₂₀Cr alloy showed comparatively better pitting resistance.

4.4 General discussion

Nanocrystalline metals are reported to have increased adsorption capabilities [2,36,37]. According to adsorption theory of passivity as proposed by Frumkin [38] and supported by Uhlig [39-41], inhibition of the anodic process are regarded as being due to adsorption of atoms of oxygen (or other atoms) which retarded the anodic process of metal dissolution. Increased adsorption of oxygen on nanocrystalline alloys therefore may be one of the reasons of increased passivation ability, i.e., lower critical current density and more negative passivation potential.

However, more recently, the point defect model (PDM) as proposed by Macdonald and co-workers [42,43] described the growth and breakdown of passive film from a microscopic perspective. This model is based on the assumption that the passive film contains a high concentration of point defects, such as oxygen vacancies and metal cation vacancies. Generation and annihilation of these vacancies also occurs on the metal/film interface which is influenced by the substrate material. The growth and breakdown of the passive film involves migration of these point defects under the influence of the electrostatic field in the passive film. Thus, the key parameters in determining the transport of point defects and hence the kinetics of film growth is the density and the diffusivity of the defects in the passive film. These parameters can be determined by Mott-Schottky analysis. Meng et al. [9] reported formation of an n type passive film on both nc and mc alloys where the donor density of the passive film formed on nanocrystalline alloys was found to be significantly less than that of microcrystalline alloys which indicated improved passivation behaviour (i.e., enhanced resistance to passive film destruction) of nanocrystalline alloys. However, a p-n type passive film was reported by Ye et al. [11] where the density of donor and acceptor did not change significantly. Therefore, detailed

Mott-Schottky analysis in conjunction with PDM may be a powerful tool in understanding the effect of nanocrystalline structure on the passivation behaviour of FeCr alloys in the future.

It was reported that nanocrystalline surfaces possess lower electron work function (EWF) than microcrystalline surfaces and also adhesive forces increase with decreases in the EWF [44]. This indicates that the passive film formed on the nanocrystalline surface possess enhanced adhesion strength between passive film and the alloy surface due to the increase in the electron activity at grain boundaries and possible pegging of the passive film in to the grain boundaries [12,44]. Increased adhesive strength may lead to improved passivating ability of the alloy as observed in the current study.

The findings presented in this paper may possibly contribute towards meaningful implications regarding the development of more corrosion resistant stainless steel with lower Cr content if the associated production processes can be up scaled. Further, the effect of nanocrystalline structure on the properties may differ by several orders of magnitude if the grain size is reduced further to ~10 nm or less as the volume fraction of triple points increases sharply with grain refinement [30]. With the help of improved processing techniques, it was possible to develop artefact free nanocrystalline Fe-Cr based alloys with the grain size of less than 10 nm [45,46]. Further investigations, comparing the effect of such fine grain size (<10 nm) on corrosion behaviour of Fe-Cr alloys will be reported in the subsequent publications.

4. CONCLUSIONS

Nanocrystalline and microcrystalline Fe₂₀Cr alloys were successfully prepared by ball milling followed by annealing, compaction and sintering. The passivation behaviour of nc and mc Fe₂₀Cr alloys as tested in the two solutions using potentiodynamic polarization test established that grain refinement (to the nanometer scale) led to substantial improvement in the passivation behaviour, and that the pitting resistance was also substantially improved.

The enhanced passivation behaviour and pitting resistance of nanocrystalline Fe₂₀Cr alloy were attributed to the formation of a passive surface film richer in Cr. This Cr enrichment of the passive film formed upon the nanocrystalline alloy surface in the two solutions was confirmed using XPS and SIMS analysis. Some possible mechanisms of Cr enrichment of the passive film formed on the nanocrystalline alloy were proposed.

ACKNOWLEDGEMENTS

Financial support from the Australian Research Council (ARC) with grant (DP0665112) and Australian Research Network for Advanced Materials (ARNAM) is gratefully acknowledged. We thank A/Prof Nick Birbilis and Prof R.C. Newman for useful discussions. The authors are also thankful for support of Australian Institute of Nuclear Science and Engineering (AINSE) and La Trobe University for carrying out the SIMS and XPS work respectively.

References

1. M.A. Meyers, A. Mishra, D.J. Benson, *Prog. Mater. Sci.*, 51 (2006) 427.
2. H. Gleiter, *Prog. Mater. Sci.*, 33 (1989) 223.
3. R.K.S. Raman, R.K. Gupta, C.C. Koch, *Philos. Mag.*, 90 (2010) 3233.
4. R.K. Gupta, R.K.S. Raman, C.C. Koch, *J. Mater. Sci.*, 45 (2010) 4884.
5. K.D. Ralston, N. Birbilis, *Corrosion*, 66 (2010) 0750051.
6. H. Kaesche, *Corrosion of metals : physicochemical principles and current problems*, Springer, New York (2003).
7. P.F. King, H. Uhlig, *J. Electrochem. Soc.*, 63 (1959) 2026.
8. H.H. Uhlig, *Corros. Sci.*, 19 (1979) 777.
9. G. Meng, Y. Li, F. Wang, *Electrochim. Acta*, 51 (2006) 4277.
10. C.T. Kwok, F.T. Cheng, H.C. Man, W.H. Ding, *Mater. Lett.*, 60 (2006) 2419.
11. W. Ye, Y. Li, F. Wang, *Electrochim. Acta*, 51 (2006) 4426.
12. X.Y. Wang, D.Y. Li, *Electrochim. Acta*, 47 (2002) 3939.
13. A.Q. Lü, Y. Zhang, Y. Li, G. Liu, Q.H. Zang, C.M. Liu, *Acta Metall. Sin.*, 19 (2006) 183.
14. B.N. Mordyuk, G.I. Prokopenko, M.A. Vasylyev, M.O. Iefimov, *Mat. Sci. Eng. A*, 458 (2007) 253.
15. T.H.D. Keijster, J.I. Longford, E.J. Mittemeijer, A.B.P. Vogel, *J. Appl. Crystallogr.*, 15 (1982) 308.
16. R. Gupta, R.K.S. Raman, C.C. Koch, *Mat. Sci. Eng. A*, 494 (2008) 253.
17. R. Kirchheim, B. Heine, H. Fischmeister, S. Hofmann, H. Knote, U. Stolz, *Corros. Sci.*, 29 (1989) 899.
18. A. Tschöpe, R. Birringer, *Acta Metall. Mater.*, 41 (1993) 2791.
19. K. Lu, R. Luck, B. Predel, *Mat. Sci. Eng. A*, 179-180 (1994) 536.
20. R. Kirchheim, X.Y. Huang, P. Cui, R. Birringer and H. Gleiter, *Nanostruct. Mater.*, 1 (1992) 167.
21. B. Yu, P. Woo, U. Erb, *Scripta Mater.*, 56 (2007) 353.
22. L. Wang, J. Zhang, Y. Gao, Q. Xue, L. Hu, T. Xu, *Scripta Mater.*, 55 (2006) 657.
23. V. Afshari, C. Dehghania, *Corros. Sci.*, 51 (2009) 1844.
24. S.G. Wang, C.B. Shen, K. Long, T. Zhang, F.H. Wang, Z.D. Zhang, *J. Phys. Chem. B* 110, (2006) 377.
25. O. El Kedim, S. Paris, C. Phigini, F. Bernard, E. Gaffet, Z.A. Muni, *Mat. Sci. Eng. A*, 369 (2004) 49.
26. O. El Kedim, H. S. Cao, D. Guayc, *J. Mater. Process. Tech.*, 121 (2002) 383.
27. Z.B. Wang, N.R. Tao, W.P. Tong, J. Lu, K. Lu, *Acta Mater.*, 51 (2003) 4319.
28. I. Kaur, W. Gust, L. Kozma, *Handbook of grain and interphase boundary diffusion data: Stuttgart: Ziegler Press*, (1989) 523.
29. A.W. Bowen, G.M. Leak, *Metall. Trans.*, 1 (1970) 1695.
30. G. Palumbo, S.J. Thorple, K.T. Aust, *Scripta Metall. Mater.* 24 (1990) 2347.
31. H. Fischmeister, U. Roll, *Z. Anal. Chem.* 319 (1984) 639.
32. K. Asami, K. Hashimoto, S. Shimodaira, *Corros. Sci.*, 19 (1978) 151.
33. P. Brusech, K. Muller, A. Atrens, H. Neff, *Appl. Phys.* 38A (1985) 1.
34. C. Leygraf, G. Hullquest, V.H. Knyazheva, A.V. Plaskeyev, Y.M. Kolotyarkin, *Corros. Sci.*, 19 (1979) 343.
35. A.J. Sedriks, *Corrosion of stainless steels*, 2nd . New York : Wiley (1996)
36. H. Zhang, R. L. Penn, R. J. Hamers, J. F. Banfiel, *J. Phys. Chem. B*, 103 (1999) 4656
37. C. Lemier, J. Weissmuller, *Acta Mater.*, 55 (2007) 1241.
38. A.N. Frumkin, W.C. Bagotskii, Z.A. Jofa, B.N. Kabanov, *Kinetika elektrodynk protsessov Kinetics of Electrode Processes*, *Moskov. Gos. Univ.* (1952).
39. H.H. Uhlig, *Corrosion Handbook*, New York (1948).
40. H.H. Uhlig, *Corrosion and Corrosion Control*, New York (1963).
41. H.H. Uhlig, P.F. King, *J. Electrochem. Soc.*, 106 (1959) 1.

42. C.Y. Chao, L.F. Lin, D.D. Macdonald, *J. Electrochem. Soc.*, 128 (1981) 1191.
43. C.Y. Chao, L.F. Lin, D.D. Macdonald, *J. Electrochem. Soc.*, 128 (1981) 1194.
44. S. Tao, D. Y. Li, *Nanotechnology* 17 (2006) 65.
45. R.K. Gupta, K.S. Darling, R.K. Singh Raman, K.R. Ravi, C.C. Koch, B.S. Murty, R.O. Scattergood, *J. Mater. Sci.*, 47 (2012) 1562. (DOI 10.1007/s10853-011-5986-6).
46. R.K. Gupta, R.K. Singh Raman, C.C. Koch, *TMS 2008 Annual Meeting*, 1 (2008) 151.